

Core collapse supernova remnants with ears

Aldana Grichener¹ and Noam Soker¹

ABSTRACT

We study the morphologies of core collapse supernova remnants (CCSNRs) and find that about third of CCSNRs have two opposite ‘ears’ protruding from their main shell, and that the typical energy that is required to inflate these ears is about 10 percents of the explosion kinetic energy. We argue that these properties are most compatible with the expectation from the explosion jet feedback mechanism (JFM). Based on previous studies of ears in CCSNRs and the similarity of some ears to those found in planetary nebulae, we assume that the ears are inflated by jets that are launched during the explosion, or a short time after it. In the JFM explosion process the last jets’ launching episode takes place just after the core has been ejected. These jets expand freely, interact with the exploding gas at some distance from the center, and form the ears. Under simple geometrical assumptions we find that the extra kinetic energy of the ears is in the range of 1 to 10 percents of the explosion energy. As not all of the kinetic energy of the jets ends in the ears, we estimate that the typical kinetic energy in the jets that inflated the ears is about 5 to 15 percents of the explosion energy. This study further supports the call for a paradigm shift from neutrino-driven to jet-driven core-collapse supernova mechanisms.

1. INTRODUCTION

In the explosion of core-collapse supernovae (CCSNe) a huge amount of gravitational energy is released when the inner part of the core collapses to form a Neutron Star (NS) or a Black Hole (BH). There are two contesting proposed processes for channelling this gravitational energy to the exploding star. The older one and much better studied is the delayed neutrino mechanism (Wilson 1985 and Bethe & Wilson 1985, and, e.g., Janka et al. 2016, and Müller 2016 for reviews). The second one is the jet-feedback mechanism (JFM; Soker 2016b), where the jittering-jets mechanism (e.g., Papish & Soker 2011, 2014a,b; Gilkis & Soker 2014, 2015, 2016) operates in most regular CCSNe, and well collimated jets operate in super-energetic CCSNe (Gilkis et al. 2016; Gilkis 2016). From polarization measurements Maund et al. (2007) find departure from axial symmetry in the Type Ib/c SN 2005bf. They attribute it to a Nickel-56 rich jet whose axis is tilted with respect to the axis of the photosphere, that has penetrated the CO core, but not the He mantle. The jittering-jets mechanism accounts for such jets. Polarimetric observations of SN 2015bn that indicate an elongated morphology further support the presence of jets in CCSNe (Inserra et al. 2016)

There is an alternative scenario where the explosion energy of massive stars originates in the nuclear burning of helium with oxygen (Burbidge et al. 1957). However, the rapid pre-collapse core rotation that is required for this scenario to work (Kushnir 2015) will lead to the launching of jets that carry much more energy than that released by the thermonuclear burning (Gilkis et al. 2016).

There are three lines of arguments to support the operation of the JFM in the explosion of massive stars (Soker 2016b). (1) Observations show that most CCSNe explode with a typical energy (mainly the

¹Department of Physics, Technion – Israel Institute of Technology, Haifa 32000, Israel; aldanag@campus.technion.ac.il; soker@physics.technion.ac.il

kinetic energy), that is about equal to and up to several times the binding energy of the ejected mass, $E_{\text{explosion}} \simeq \text{few} \times E_{\text{bind}} \approx 10^{51}$ erg. This hints at the operation of a negative feedback mechanism.

(2) The presence of jets in long gamma ray bursts (GRBs; e.g., Woosley 1993; Shaviv & Dar 1995; Sari & Piran 1997). Some long GRBs are observed to be associated with Type Ic supernovae (e.g., Cano et al. 2016), showing that jets can be produced at the collapse. In addition there are claims for a real jet in the SN remnant (SNR) Cassiopeia A (Fesen & Milisavljevic 2016), and observations for a significant role played by jets in at least some CCSNe (e.g. Lopez et al. 2011, 2013, 2014; Milisavljevic et al. 2013; González-Casanova et al. 2014).

(3) The 32 years old delayed neutrino mechanism encounters three problems (Papish et al. 2015). (i) In the delayed-neutrino mechanism the explosion starts with the revival of the stalled shock of the inflowing core gas. This is not always achieved in numerical simulations, even in the most sophisticated ones. (ii) Even if the stalled shock is revived, in most simulations the desired energy of $\approx 10^{51}$ erg is not achieved. (iii) When in simulations based on neutrino-driven explosion the explosion energy is scaled to observed CCSNe, such as SN 1987A, the maximum energy that the delayed-neutrino mechanism can supply is about 2×10^{51} erg (e.g., Sukhbold et al. 2016; Sukhbold & Woosley 2016). Even when convection-enhanced neutrino-driven explosion is considered (convective-engine) the explosion energy cannot get higher than this limit (Fryer et al. 2012). Therefore, the delayed neutrino mechanism cannot account for super energetic CCSNe (SESNe).

Jet-driven explosions of CCSNe have been studied over the years (e.g. LeBlanc & Wilson 1970; Meier et al. 1976; Bisnovatyi-Kogan et al. 1976; Khokhlov et al. 1999; MacFadyen et al. 2001; Höflich et al. 2001; Woosley & Janka 2005; Burrows et al. 2007; Couch et al. 2009, 2011; Takiwaki & Kotake 2011; Lazzati et al. 2012; Mösta et al. 2014; Bromberg & Tchekhovskoy 2016). The constant direction of the jets in these studies requires that there will be a well defined angular momentum axis, implying that the pre-collapsing core has a rapid rotation. These are rare cases, and they do not operate via an efficient JFM. It seems that jets are more common than what the initial conditions in these studies require, and more in line with the JFM for exploding CCSNe.

Castelletti et al. (2006) suggest that the SNR Puppis A with a morphology that contains two opposite ‘ears’, was shaped by jets. Such jets might be the last two opposite jets launched in the jittering jets mechanism, or the signature of well collimated long-lived double jets. Two opposite ears are observed also in Type Ia SNR (SNR Ia). Tsebrenko & Soker (2015a) list such SNR Ia, and study the formation of such opposite ears by jets. In section 2 we discuss the relation between jets and ears. In section 3 we list SNRs of CCSNe where we identified ears, and in section 4 we estimate the energy that is needed to inflate such ears if they are formed during, or shortly after, the explosion. Tsebrenko & Soker (2015a) list SNRs of Type Ia SNe (SNR Ia) that have ears. In section 5 we discuss our results and compare with ears in SNR Ia.

2. THE RELATION BETWEEN JETS AND EARS

A protrusion from the main SNR shell that possesses one or more of the following properties will be referred to as an ‘ear’. (1) It has a different characteristics than the main SNR shell. Examples include a substantially different ratio of radio to X-ray surface brightness, or that the ear is disconnected from the main SNR shell by a faint region. (2) In a case that the SNR shell has a general elliptical appearance, the protrusion is along the long axis of the SNR. (3) There are two opposite protrusions with respect to the center of the SNR.

There are three types of interactions that can in principle lead to the formation of two opposite ears by

jets in the SNR. Note that in many cases we might observe only one of the two ears. (1) Pre-explosion ears in the circumstellar matter (CSM). The spherical explosion gas fills the CSM shell, and the imprint of ears survives to the SNR phase. This can be the case if the progenitor is in a binary system, and a mass transfer leads the mass-accreting companion to launch jets. These jets form ears in the CSM before explosion. (2) Jets that are launched during the explosion. (3) Post-explosion jets that are launched by the remnant, either a NS or a BH. These jets can be launched shortly after the explosion or a long time after, e.g., in a PWN. For example, in a recent paper Olmi et al. (2016) conducted a 3D simulation of a PWN and demonstrated the formation of jets. In all three scenarios the jets are not active during the SNR phase, unless a close binary companion transfers mass to the compact remnant (see below).

In SN Ia the exploding white dwarf (WD) does not survive. Hence, only the first two possibilities might account for ears in SNR Ia. Tsebrenko & Soker (2013) conducted hydrodynamical simulations and demonstrated that both pre-explosion and during-explosion jets can in principle form the ears that are observed in SNR Ia. It is not clear yet how an exploding WD can launch jets, i.e., it might require a rapidly rotating WD. For that, Tsebrenko & Soker (2015a) and Tsebrenko & Soker (2015b) prefer the pre-explosion ear scenario to account for ears in SNR Ia.

In CCSNe all three types of processes for the formation of ears can in principle operate. The bipolar structure of the three rings around SN 1987A demonstrates that the CSM of a CCSN can have an axisymmetrical structure, most likely formed by a strong binary interaction that involves a merger process (e.g., Morris & Podsiadlowski 2009). In the specific case of SN 1987A the binary system merged long before the explosion (e.g., Chevalier & Soker 1989; Podsiadlowski et al. 1990). In the case of a merger, the pre-explosion star is likely to possess a relatively rapid rotation. This increases the likelihood of the formation of an accretion disk around the newly born NS, and hence of the launching of jets (e.g., Gilkis 2016).

The relation between jets and ears in CCSNRs was mentioned in the past in relation to several SNRs (e.g., Dubner & Giacani 2015). Gaensler et al. (1998) noted the similarity of the ears in the SNR G309.2-00.6 with those in the SNR W50, and suggested they were formed by jets launched from the remnant. Castelletti et al. (2006) suggested that the nice ears of Puppis A (e.g., Reynoso & Walsh 2015) were shaped by jets. Hwang et al. (2004) observed the two opposite Si-rich and Fe-poor jets in Cassiopeia A. They comment that the bipolar structure is due to jets during the explosion, rather than to pre-explosion cavities in the CSM.

We show the X-ray and radio images of SNR Cassiopeia A in Fig. 1. Only the eastern jet and ear are clearly seen. There is a Si-rich counter jet more or less where we mark the western ear (Hwang et al. 2004), that supports the notion that there is a counter ear. The X-ray image presents a bright outer region (in green) which marks the location of a shock wave generated by the SNR expansion. The eastern ear is clearly seen by this thin green region, and the radio image.

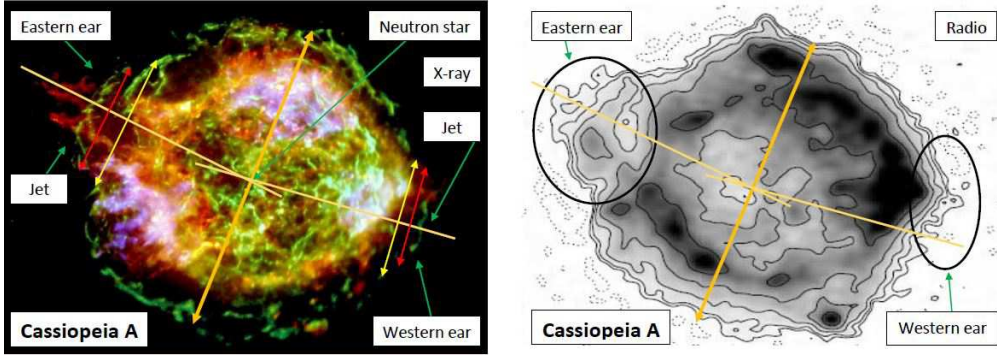


Fig. 1.— Images of the SNR Cassiopeia A. Left: An X-ray image taken from the chandra gallery (based on Hwang et al. 2004). Red, blue and green represent Si He α (1.78-2.0 keV), Fe K (6.52-6.95 keV), and 4.2-6.4 keV continuum, respectively. Right: A radio image at 69 MHz obtained from a single 0.2 MHz sub-band, as published by Oonk et al. (2016). We added arrows to indicate different quantities that we will use in our analysis in section 4.

The eastern jet-ear structure of the SNR Cassiopeia A clearly demonstrates the relation between a jet that was launched during the explosion (Hwang et al. 2004) and the presence of an Ear. In this case the jet penetrated the SNR shell and its head precedes the ear. In some other cases the jet might not penetrate the SNR shell, and its material is enclosed within the ear and SNR shell. If we are to learn from SNR Cassiopeia A, then the presence of ears support the significant role that jets play in the explosion mechanism of CCSNe.

The X-ray binary system SS433 and its associated SNR W50 (SNR G039.7-02.0) is a whole different story. Although it is not the type of objects we study, we present it here to further emphasize the relation between jets that are launched by a NS or a BH, and the presence of ears. In this system a binary companion transfers mass to the NS (or BH) remnant of the CCSN, and the accretion disc around the compact object launches relativistic jets. As can be seen in Fig. 2, the two ears occupy much of the volume of this SNR. Most of the power from the jet seems to go into the mechanical energy, producing the ears (Safi-Harb & Petre 1999).

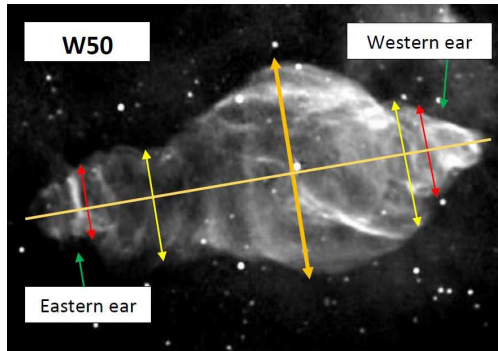


Fig. 2.— The SNR W50 in radio continuum at 1415 MHz as observed with the VLA (from Dubner et al. 1998). We added arrows to indicate different characteristic quantities of the SNR that we define in section 3.

In the systems we study there is no mass transfer from a companion. Nonetheless, the general structure of the ears in W50 is similar to the ears in the SNR G309.2-00.6 that we study later on (Gaensler et al. 1998). This suggests that the ears in SNR G309.2-00.6 were formed by jets that were launched during the explosion, or shortly after the explosion, as there are no active jets there anymore.

The main point of this section is the strong relation between the operation of jets, at present or in the past, and the presence of ears in SNRs. The morphologies of the ears we study, namely, that they are distinguish from the main SNR shell in a clear way, suggest to us that most of the ears were blown from the SNR shell, and are not just an elongation of the SNR. We therefore assume in the present study that the ears were inflated by jets, and are not the result of magnetic fields of the Pulsar Wind Nebula (PWN) as suggested by, e.g., Begelman & Li (1992).

As we cannot study the operation of jets in the past, we turn to study the ears that are observed in SNRs, and the implication of their properties on the jets that formed them and on the explosion mechanism of CCSNe.

3. SUPERNOVA REMNANTS WITH EARS

In this section, we present images of CCSNRs with ears. We examined images of 41 different CCSNRs in the Milky Way and in the Magellanic clouds. Out of these 41 CCSNRs, for 28 (not including W50) the images are clear enough to tell whether ears exist or not. We found that eight CCSNRs (not including the CCSNR W50) have distinct ears, while another four CCSNRs might have ears. Seven of CCSNR who possess ears have 2 prominent ears, and only one of them (the Crab Nebula) has one ear. If the symmetry axis, i.e., the line joining the two counter ears, is close to our line of sight, the ears will be projected on the main SNR shell and we might not see them. Therefore, the true fraction of CCSNRs with ears might be larger than the fraction of $8/28 = 29\%$ to $12/28 = 43\%$ we find here. At this stage we can say that at least about third of CCSNRs possess one or two ears.

Under the assumption that ears were shaped by jets, we set a goal to calculate the extra energy that was required to form each ear. For that, we define some geometrical properties of the ears as follows. Although the ears are not spherical, we define a diameter for each ear, and mark it with a double-headed red arrow. If a symmetry axis exists, the double-headed red arrow is more or less perpendicular to this axis. We define the base of the ear as the region on the SNR main shell from which the ear protrude. We cannot tell from the images what the shape of the base is. We assume it is circular. With a yellow double-headed arrow we mark the diameter of the base of the ear on the SNR main shell. There are large uncertainties in the exact values of the diameters of the ears and bases. Nonetheless, we think they are adequately defined for our purpose of estimating the extra energy that is needed to inflate the ears. This calculation is postponed to section 4. We also define a diameter for the SNR shell, or a typical size if the SNR substantially departs from a spherical geometry, and mark it with a double-headed thick orange arrow. In some cases we also mark the symmetry axis of the SNR.

In most images we were consistent with the colors of the arrows mentioned above. Nevertheless, in some cases, in order to stress the arrows over the background, we used different colors. In the image of Vela SNR we marked the radius of the ear with a double-headed purple arrow, the radius of the base with a double-headed brown arrow and the radius of the SNR itself with a double-headed thick blue arrow. In the image of SNR G309.2-00.6, we marked the base radius of the overlapping area with a double-headed bourdeaux arrow, and in the image of Puppis A we stressed the radius of the eastern ear using a white

broken line.

We will not discuss the different CCSNRs, but only refer to the ears and the quantities that are relevant to our study.

SNR 3C58. There is a rich literature on this SNR (e.g., Slane et al 2004; López-Coto et al 2016), but as stated above, we limit our study to the morphology of the ears. Its image is presented in Fig. 3, together with its PWN. This CCSNR has two opposite ears on the long axis of the SNR. The eastern ear is significantly larger and clearer than the western ear. We present two panels to better mark morphological parameters for each ear (the diameter of the ear and the diameter of the ear’s base). The pulsar J0205+6449 at the center of the SNR launches two opposite jets along the symmetry axis (e.g., Shibano et al. 2008).

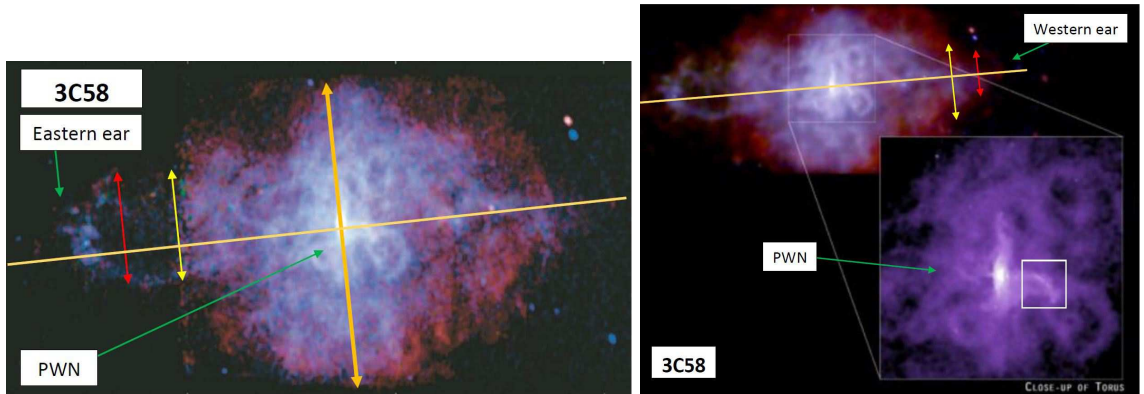


Fig. 3.— The SNR 3C58. ACIS/Chandra images of 3C58 in the energy bands 0.5–1.0 keV (red), 1.0–1.5 keV (green), and 1.5–10 keV (blue). Both panels are based on Slane et al (2004); right image was taken directly from the Chandra gallery. The images do not have the same scale.

SNR Puppis A. In Fig. 4 we present the well studied (e.g., Dubner et al. 2013) oxygen rich SNR Puppis A. The two small ears are clearly resolved in these images, and despite that the SNR has no symmetry axis, the two opposite ears are prominent. Castelletti et al. (2006) and Dubner & Giacani (2015) already mentioned that the ears could have been formed by jets. Reynoso & Walsh (2015) suggested that the asymmetry of the two ears results from asymmetrical interaction with the interstellar medium (ISM). Because of the lack of symmetry, we draw a separate ‘symmetry-axis’ for each ear.

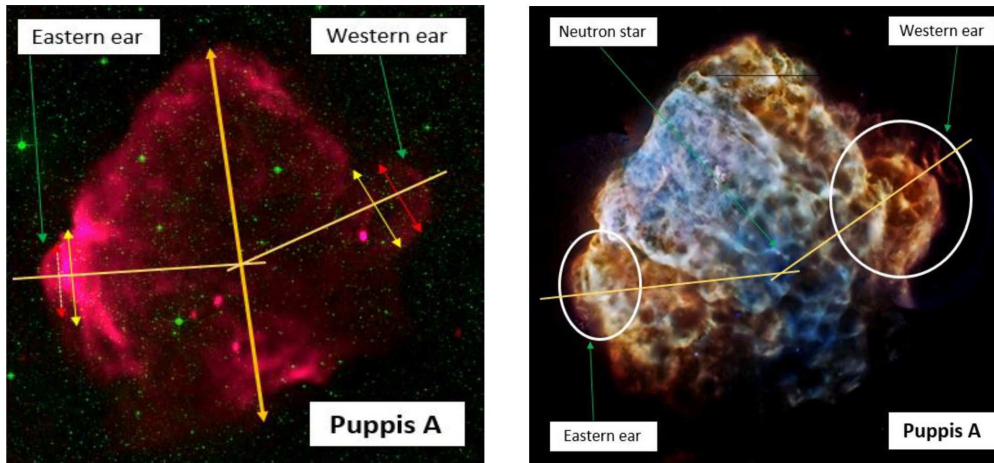


Fig. 4.— The SNR Puppis A. Left: The composite picture displays the radio continuum emission (pink) obtained by combining Parkes and broadband ATCA observations, with a visible light (green) background from the Digital Sky Survey. The image was reproduced by E. Reynoso at ATNF Daily Astronomy Picture from the paper Reynoso & Walsh (2015). Right: A full view of Puppis A in X-ray, where red, green, and blue correspond to the 0.3-0.7, 0.7-1.0, and 1.0-8.0 keV bands, respectively (from Dubner et al. 2013).

SNR Semeis 147. In Fig. 5 we present the image of Semeis 147. The shell has a general circular morphology, but with obvious blow-outs in the eastern and western direction, i.e., the ears. Those elongations define a bilateral axis passing through the center (e.g., Ng et al. 2007; Gvaramadze 2006). The SNR contains a central pulsar, PSR J0538+2817. Ng et al. (2007) attribute the asymmetrical expansion of this SNR to inhomogeneities in the surrounding interstellar medium. Gvaramadze (2006) claims that a possible explanation to the extended morphology is that Semeis 147 is a remnant of a SN which exploded within a low density bubble surrounded by a shell. The bubble was formed by the stellar wind of the SN progenitor during its WR phase of evolution. Dinçel et al. (2015) raise the possibility that the elongation of Semeis 147 is due to the jets or the torus of the PWN. Dinçel et al. (2015) further suggest that the progenitor was an interacting binary system. As we discussed in section 2, such a binary interaction might form pre-explosion ears. In this study we assume that the ears were formed by jets launched during the explosion or shortly after the explosion.

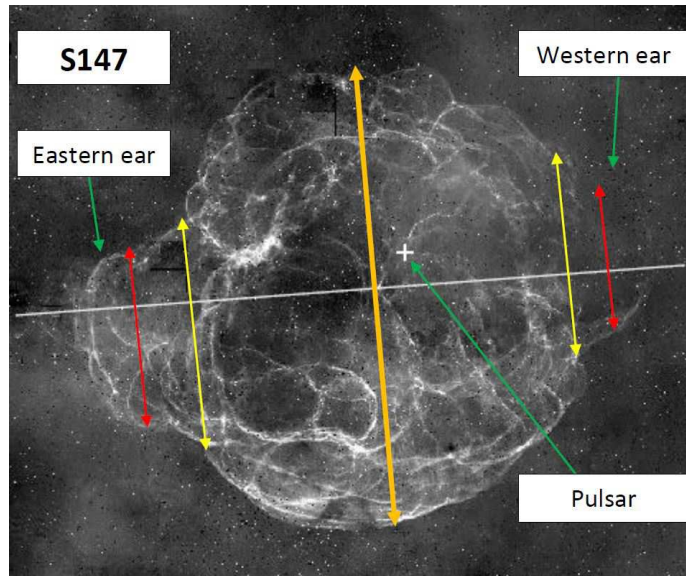


Fig. 5.— An $H\alpha$ image of the SNR Semeis 147 taken from Gvaramadze (2006) who reproduced an image from Drew et al. (2005). The symmetry axis is from the original image.

The Vela SNR. In Fig. 6 we present the Vela SNR. The Vela SNR possesses many protrusions from its main shell. Aschenbach et al (1995) labeled some of these protrusions, as can be seen in the figure. We added the black ellipses to mark the ears and the morphological quantities that are relevant to our study. The bright clump is a separate SNR, Puppis A. Miceli et al. (2013) refer to the protrusions as detached clumps, and simulate the formation of the eastern ear with a dense clump that was formed during the explosion (i.e., not with a pulsar wind). The kinetic energy of the dense clump in their simulations is about 5% of the kinetic energy of the SNR shell. We accept their general view on the formation of the eastern ear, but attribute the formation of ears to jets, rather than to clumps. The outcome of a jet and a clump long after the jet has ceased is similar. Gvaramadze (1999), on the other hand, attribute the structure of the Vela SNR to the interaction of the SN ejecta with a bubble blown prior to the explosion, accompanied by Rayleigh-Taylor instabilities. The Vela SNR contains a central pulsar (PSR 0833-45; marked with a small black cross) and a long collimated jet-like structure (e.g., Grondin et al 2013).

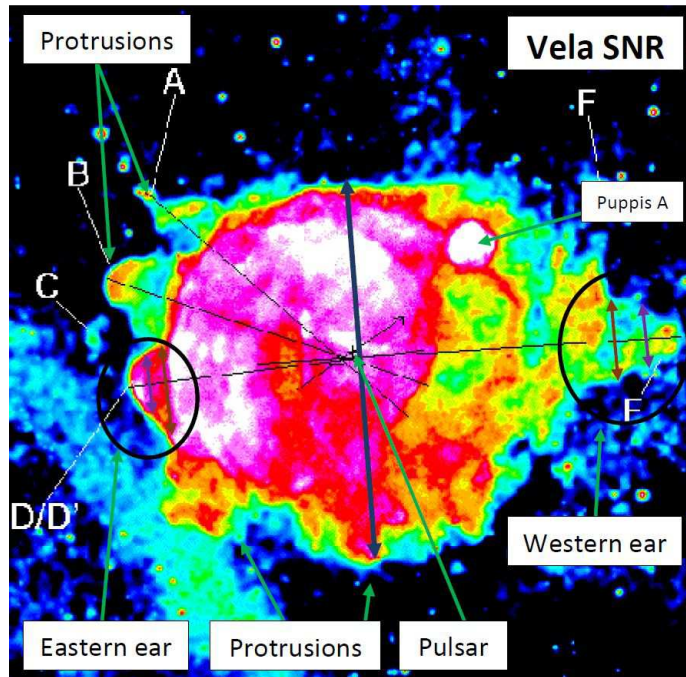


Fig. 6.— The Vela SNR. This is a ROSAT all-sky survey image (0.1–2.4 keV) from Aschenbach et al (1995). The black lines, including the symmetry axis (the longest one), and the letters marks on the protrusions are from there as well. We added the black ellipses to mark the location of the ears. The two double-headed arrows in purple mark the diameter of the ears, while the blue-thick double-headed arrow marks the diameter of the SNR shell. The two double-headed brown arrows represent the diameter of the base of the ears.

SNR G309.2-00.6. We present the radio image of this SNR in Fig. 7. The geometrical quantities relevant to our study are marked on the figure. This CCSNR has two clear ears as we mark on Fig. 7. Gaensler et al. (1998) note the similarity between the ears in this SNR and those in SNR W50, and discuss the formation of the ears by jets launched by the remnant. Despite the resemblance between the morphologies of SNR G309.2-00.6 and SNR W50, there is no evidence of a binary companion to the remnant of SNR G309.2-00.6 and no evidence for jets (Safi-Harb et al. 2007).

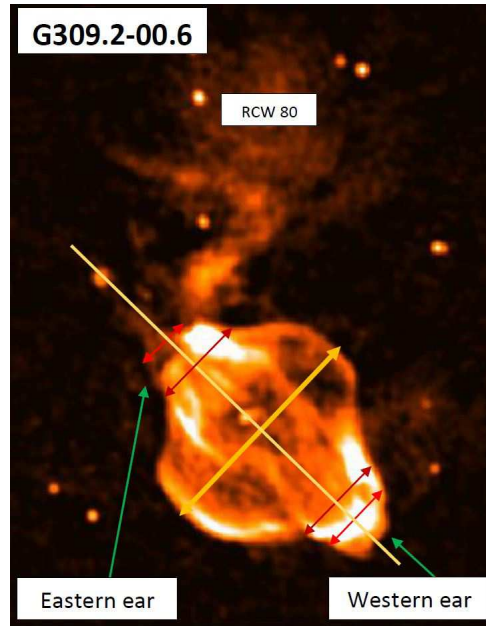


Fig. 7.— The SNR G309.2-00.6. In the background lies the emission nebula RCW 80. The radio image is taken from the site of the School of Physics, The university of Sydney, where it was posted as production from Gaensler et al. (1998).

SNR W44. The image of SNR W44 is presented in Fig. 8, together with our drawing of the relevant geometrical quantities of the ears. It contains a central pulsar, PSR B1853+01, which has a PWN that emits radio and X-ray (e.g., Shelton et al 2004). This SNR has the appearance of a non-circular shell elongated in the south-east and north-west directions (e.g., Tanaka 2009; Castelletti et al. 2007). Those elongations are the ears that we study.

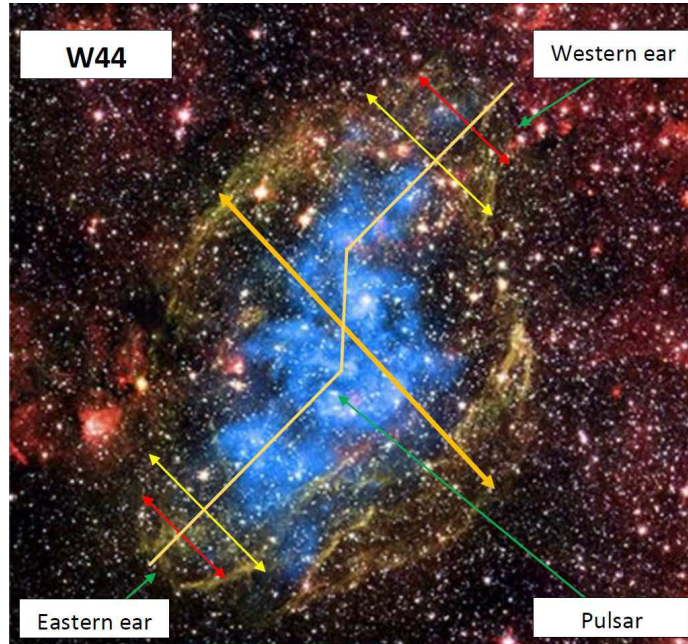


Fig. 8.— The SNR W44. Composite image taken from the Chandra gallery. The cyan represents X-ray (based on Shelton et al 2004), while the red, blue and green represent infra-red (based on NASA/JPL-Caltech). We added three beige thick lines to schematically define the S-shape of this SNR.

The Crab Nebula. Fig. 9 presents one of the best studied SNR. Several protrusions are clearly resolved, including an eminent pillar. We can clearly identify only one ear, as marked on the figure. The ear is qualitatively different from the other protrusions. It is along the long axis of the SNR, there is a sharp drop in surface brightness from the SNR shell to the ear, and the geometry of the ear is more spherical and not a continuation of the edge of the main SNR shell. The diameter of the ear and the diameter of its base almost overlap because the ear geometry is almost a half-sphere.

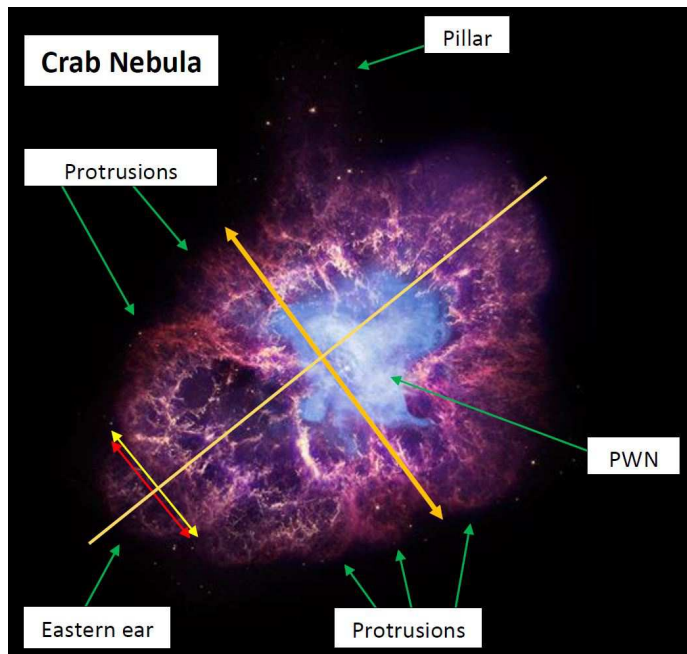


Fig. 9.— The Crab Nebula. The composite image is assembled from X-ray (Blue), Optical (Red-Yellow) and Infrared (Purple). The image was taken from Chandras gallery. The X-ray is based on (Seward et al. 2006), the Optical is based on NASA/ESA/ASU/J.Hester and A.Loll and the Infrared is based on NASA/JPL-Caltech/Univ.

At the center of the Crab Nebula there is a pulsar with its PWN (e.g., Hester et al. 2002; Temim et al. 2006; Seward et al. 2006). As mentioned by Komissarov & Lyubarsky (2003) and Lyubarsky (2012), most of the energy of the pulsar is expelled in the equatorial plane, and not along the polar directions. A PWN might form two opposite ears by the pinching effect of the toroidal magnetic field (e.g., Begelman & Li 1992), but as we discussed in section 2, we instead discuss the formation of ears by jets.

Schenck et al (2014) detect a faint protrusion to the northeast of the CCSNR B004973.6, and term it an ear. This protrusion does not comply with our definition of an ear. We therefore consider the presence of ears in this SNR as questionable. There are three other CCSNRs that have general morphology that we consider as compatible with the presence of ears, but where we see no ears at present. These are SNR 0540-69.3, RCW 103 and W49B. Bear & Soker (2017) for example, compare the structure of SNR W49B with that of several planetary nebulae, some of them have ears.

Together with the 8 CCSNe we presented in sections 2 and 3 (not including W50), we conclude that 8-12 out of the 28 CCSNRs with well resolved images have ears. This, together with projection effects that can hide ears in some CCSNRs, is the source of our estimate that at least third of CCSNRs have (or had) ears.

4. ESTIMATING THE ENERGY TO INFLATE EARS

We calculate the approximate fraction of the energy that was required to inflate each ear under the following assumptions. (1) Before the jets formed the ears, the SNR shell was spherical. (2) As well, the mass density per unit area on the shell was constant. (3) The mass in the jet is small relative to the mass of the SNR that the jet interacted with and is now part of the ear. This holds if the velocity of the jets was much higher than that of the shell, as we assume here. (4) The ear was formed during, or shortly after, the explosion. (5) The ear has a more or less spherical shape. This is definitely not the case, but it is adequate to our goals when the other uncertainties are considered. (6) The velocity of the SNR shell and the ear did not change much since the formation of the ear.

Under assumption 2 the ratio between the mass in the ear, M_{ear} , and the total mass in the SNR, i.e., including the ear mass, M_{SNR} , is

$$\mu \equiv \frac{M_{\text{ear}}}{M_{\text{SNR}}} = \frac{1 - \cos \theta}{2} = \frac{1}{2} \left[1 - \sqrt{1 - \left(\frac{R_{\text{base}}}{R_{\text{SNR}}} \right)^2} \right], \quad (1)$$

where the radius of the SNR, R_{SNR} , and the radius of the base of the ear, R_{base} , are half the lengths of the double-headed thick orange arrows and yellow arrows in the images presented in sections 2 and 3, respectively, and θ is the half opening angle of the ear as seen from the center of the SNR.

The average expansion velocity of the SNR and, under assumption 4, the average velocity of the ear are given by

$$v_{\text{SNR}} = \frac{R_{\text{SNR}}}{t}, \quad (2)$$

and

$$v_{\text{ear}} = \frac{R_{\text{SNR}} + R_{\text{ear}}}{t}, \quad (3)$$

where t is the age of the SNR, and the radius of the ear, R_{ear} , is half the length of the double-headed red arrows in the figures presented in section 2 and 3.

Under our assumptions the kinetic energy of the gas that is now in the ear before it was acted upon by the jet is given by

$$E_{\text{ear},0} \simeq \frac{M_{\text{ear}} v_{\text{SNR}}^2}{2}, \quad (4)$$

and the present kinetic energy of this gas is

$$E_{\text{ear}} \simeq \frac{M_{\text{ear}} v_{\text{ear}}^2}{2}. \quad (5)$$

We assume the SNR moves supersonically, and we neglect the thermal energy of the gas. We now make the assumption that the entire energy of the jets was transferred to the extra energy of the ears. This is a strong assumption, as during the interaction, dissipation heat the gas and some of the energy is radiated away. This assumption, therefore, underestimates the energy of the jet. Subtracting the kinetic energy of the gas in the ear before the interaction with the jet, $E_{\text{ear},0}$, from the kinetic energy of the ear, E_{ear} , gives an estimate of the energy that was required to inflate the ear by the jet

$$E_{\text{jet}} \approx \Delta E_{\text{ear}} = E_{\text{ear}} - E_{\text{ear},0}. \quad (6)$$

The desired quantity is the ratio, ϵ_{ear} , of this energy to that of the entire SNR shell,

$$E_{\text{SNR}} \simeq \frac{M_{\text{SNR}} v_{\text{SNR}}^2}{2}. \quad (7)$$

We find

$$\epsilon_{\text{ear}} \equiv \frac{\Delta E_{\text{ear}}}{E_{\text{SNR}}} \simeq \mu \left[(1 + \Gamma)^2 - 1 \right], \quad (8)$$

where we defined

$$\Gamma \equiv \frac{R_{\text{ear}}}{R_{\text{SNR}}}. \quad (9)$$

In Table 1 we present the result of our calculations, for each ear separately and for the two ears combined (ϵ_{ears}) for each SNR.

SNR	ϵ_{west}	ϵ_{east}	ϵ_{ears}
Cassiopeia A	0.038	0.064	0.10
3C58	0.037	0.032	0.07
Puppis A	0.009	0.010	0.02
S147	0.039	0.072	0.11
Vela	0.005	0.004	0.01
G309.2-00.6	0.039	0.03	0.07
W44	0.034	0.029	0.06
Crab Nebula	-	0.034	0.03

Table 1: The ratio of the extra energy in the ears to that in the SNR shell. The last column is the combined values of the two ears.

In the interaction of the jets with the shell, some energy might be radiated away or be spread in a larger volume than that of the ear (e.g., to the sides of the base of the ear). Our calculation does not take these effects into account. For that, the energy of the inflating jets is somewhat larger than the extra energy in the ear $E_{\text{jet}} \gtrsim \Delta E_{\text{ear}}$. As we mentioned in section 3, Miceli et al. (2013) estimated the kinetic energy of the eastern ear in Vela SNR (i.e. the clump) is about 5% of the kinetic energy of the SNR shell. According to our calculation the extra kinetic energy of the eastern ear is about 2% of the total energy of the SNR. This demonstrates that the energy in the jets might be about a factor of ≈ 2 larger than the estimated energy in the ears (derived under different assumptions). The time of interaction between the jets and the SNR shell determines not only the amount of energy that does not end in the ear, but also the exact shape of the ear. Both quantities will have to be determined by a set of numerical simulations.

At this point we only make a crude estimate. Based on the value of $\epsilon_{\text{ears}} \approx 0.01 - 0.1$ we state that the typical energy in the two opposite jets is

$$\epsilon_{\text{jets}} \equiv \frac{E_{\text{jets}}}{E_{\text{SNR}}} \approx 0.05 - 0.15 \quad (10)$$

5. DISCUSSION AND SUMMARY

We estimated the extra kinetic energy that was required to inflate ears in CCSNRs. Our definition for ears is given at the beginning of section 2. We calculated the extra energy for eight CCSNRs whose images

are presented in sections 2 and 3. For seven CCSNRs we identified two clear opposite ears, where for the Crab Nebula we could perform the calculation for only one well identified ear.

The ears can in principle be formed before the explosion, if the SN expands to a CSM with ears, during the explosion, or after the explosion. We here made the assumption that the ears have been shaped during the explosion, or shortly after it. This holds true in at least some CCSNRs. For example, it seems that the Crab Nebula does not interact with a dense CSM or ISM (e.g., Yang & Chevalier 2015). In the Cassiopeia A SNR there is an observational indication for a jet that inflated the ear (Hwang et al. 2004; see discussion in section 2).

We crudely estimated the energy that is required to inflate the ears, and present the results in Table 1. As not all the energy of the jets ends in the ears, the original energy of the jets might be somewhat larger. Over all, we crudely estimate that the original energy in the two opposite jets that inflate ears in CCSNe is a fraction of $\epsilon_{\text{jets}} \approx 5 - 15\%$ of the kinetic energy of the SNR shell (eq. 10).

Based on the eight CCSNRs where we identified ears (not including W50), and four questionable CCSNRs, we estimated the fraction of CCSNRs which possess opposite ear-like features (section 3) to be $\approx 29 - 43\%$ of CCSNRs. If the symmetry axis, i.e., the line joining the two counter ears, is close to our line of sight, the ears will be projected on the main SNR shell and we might not see them. Therefore, the true fraction of CCSNRs with ears is likely to be higher, at a value of at least third of all CCSNRs, and more likely $\approx 40\%$ of all CCSNRs.

We find that the scenario most compatible with the large fraction of CCSNRs with jet-inflated ears, and with a typical energy relative to the explosion energy of $\epsilon_{\text{jets}} \approx 5 - 15\%$, is the jet feedback mechanism (JFM; e.g., Papish & Soker 2011; Gilkis & Soker 2016; Soker 2016b). The energy of the jets of $\epsilon_{\text{jets}} \approx 5 - 15\%$ is explained by the feedback explosion process. When the jets have enough energy to unbind the core (considering that the efficiency is not 100 per cents), explosion takes place. The final activity episode of the jets takes place when the core has already been ejected. The final part of the jets expand freely to very large distance, interact with the already ejected core, and inflate the ears. In case of a slow pre-collapse core rotation the jets' axis wobble, and the explosion is termed the jittering jets explosion mechanism (e.g., Papish & Soker 2014a,b). There are several to few tens of jet-launching episodes in different directions. In each launching episode the jets carry an amount of energy of few to about few tens percents of the explosion energy. The jets of the last episode, that are launched after the ejection of the core, inflate the ears.

It might be possible that the ears are formed shortly after the explosion by jets launched from a rapidly rotating NS remnant. However, the formation of a rapidly rotating NS is most likely to be accompanied by the launching of jets (Soker 2016a), hence bringing us back to explosion by jets.

Overall, we conclude that the fraction of CCSNRs with ears and the energy that is needed to inflate the ears are compatible with the JFM explosion mechanism of CCSNe.

The general morphologies of the ears studied here are similar to those in some SNR Ia and to many ears in planetary nebulae (examples are listed by Tsebrenko & Soker 2015b). Tsebrenko & Soker (2013) and Tsebrenko & Soker (2015b) demonstrate by hydrodynamical numerical simulations that in SNR Ia jets launched long before the explosion or during the explosion can form such opposite ears. In particular, SN Ia that explodes inside a planetary nebula with ears, will have ears itself. A SN Ia inside a CSM that once was a planetary nebula is termed SNIP.

The process we propose here, of jets launched during the explosion or shortly after it, is similar in some respects to jets that shape ears in some planetary nebulae. In planetary nebulae the jets might be

formed before or after the main nebular shell (e.g., Tocknell et al. 2014). In those planetary nebulae with ears similar to those of SNRs, it is possible that the age of the jets and nebular shells is similar, and the jets have played a role in ejecting the nebula, possibly in a feedback process (e.g., Shiber et al. 2016). We hence speculate that the formation processes of ears in planetary nebulae might have some similarity to the formation of ears in CCSNRs, and in any case, both processes involve energetic jets.

This research was supported by The Rothschild Scholars Program- Technion Program for Excellence and the E. and J. Bishop Research Fund at the Technion.

REFERENCES

- Aschenbach, B., & Egger, R., & Trumper, J. 1995, *ApJ*, 373, 587
- Bear, E., & Soker, N. 2017
- Begelman, M. C., & Li, Z.-Y. 1992, *ApJ*, 397, 187
- Bethe, H. A., & Wilson, J. R. 1985, *ApJ*, 295, 14
- Bisnovatyi-Kogan, G. S., Popov, I. P., & Samokhin, A. A. 1976, *Ap&SS*, 41, 287
- Bromberg, O., & Tchekhovskoy, A. 2016, *MNRAS*, 456, 1739
- Burbidge, E. M., Burbidge, G. R., Fowler, W. A., & Hoyle, F. 1957, *Reviews of Modern Physics*, 29, 547
- Burrows, A., Dessart, L., Livne, E., Ott, C. D., & Murphy, J. 2007, *ApJ*, 664, 416
- Cano, Z., Wang, S.-Q., Dai, Z.-G., & Wu, X.-F. 2016, arXiv:1604.03549
- Castelletti, G., Dubner, G., Brogan, C., & Kassim, N. E. 2007, *A&A*, 471, 537
- Castelletti, G., Dubner, G., Golap, K., & Goss, W. M. 2006, *A&A*, 459, 535
- Chevalier, R. A., & Soker, N. 1989, *ApJ*, 341, 867
- Couch, S. M., Pooley, D., Wheeler, J. C., & Milosavljević, M. 2011, *ApJ*, 727, 104
- Couch, S. M., Wheeler, J. C., & Milosavljević, M. 2009, *ApJ*, 696, 953
- Dinçel, B., Neuhäuser, R., Yerli, S. K., Ankar, A., Tetzlaff, N., Torres, G., & Mugrauer, M. 2015, *MNRAS*, 448, 3196
- Drew, J. E., Greimel, R., Irwin, M. J., et al. 2005, *MNRAS*, 362, 753
- Dubner, G., & Giacani, E. 2015, *A&A Rev.*, 23, 3
- Dubner, G., Loiseau, N., Rodríguez-Pascual, P., Smith, M., Giacani, E., Castelletti, G. 2013, *A&A*, 555, A9
- Dubner, G. M., Holdaway, M., Goss, W. M., & Mirabel, I. F. 1998, *AJ*, 116, 1842
- Fesen, R. A., & Milosavljević, D. 2016, *ApJ*, 818, 17
- Fryer, C. L., Belczynski, K., Wiktorowicz, G., Dominik, M., Kalogera, V., & Holz, D. E. 2012, *ApJ*, 749, 91

- Gaensler, B. M., Green, A. J., & Manchester, R. N. 1998, *MNRAS*, 299, 812
- Gilkis, A., Soker, N., & Papish, O. 2016, *ApJ*, 826, 178
- Gilkis, A. 2016, arXiv:1608.05320
- Gilkis, A., & Soker, N. 2016, *ApJ*, 827, 40
- Gilkis, A., & Soker, N. 2015, *ApJ*, 806, 28
- Gilkis, A., & Soker, N. 2014, *MNRAS*, 439, 4011
- González-Casanova, D. F., De Colle, F., Ramirez-Ruiz, E., & Lopez, L. A. 2014, *ApJ*, 781, L26
- Grondin, M., & Romani, R., & Goumard, M., & Guillemot, L., & Harding, A., & Reposeur, T. 2013, *ApJ*, 774, 110
- Gvaramadze, V. V. 2006, *A&A*, 454, 239
- Gvaramadze, V. V. 1999, *Odessa Astronomical Publications*, 12, 117
- Hester, J. J., Mori, K., Burrows, D., et al. 2002, *ApJ*, 577, L49
- Höflich, P., Khokhlov, A., & Wang, L. 2001, 20th Texas Symposium on relativistic astrophysics, 586, 459
- Hwang, U., Laming, J. M., Badenes, C., et al. 2004, *ApJ*, 615, L117
- Inserra, C., Bulla, M., Sim, S. A., & Smartt, S. J. 2016, arXiv:1607.02353
- Janka, H.-T., Melson, T., & Summa, A. 2016, arXiv:1602.05576
- Khokhlov, A. M., Höflich, P. A., Oran, E. S., et al. 1999, *ApJ*, 524, L107
- Komissarov, S. S., & Lyubarsky, Y. E. 2003, *MNRAS*, 344, L93
- Kushnir, D. 2015, arXiv:1502.03111
- Lazzati, D., Morsony, B. J., Blackwell, C. H., & Begelman, M. C. 2012, *ApJ*, 750, 68
- LeBlanc, J. M., & Wilson, J. R. 1970, *ApJ*, 161, 541
- Lopez, L. A., Castro, D., Slane, P. O., Ramirez-Ruiz, E., & Badenes, C. 2014, *ApJ*, 788, 5
- Lopez, L. A., Ramirez-Ruiz, E., Castro, D., & Pearson, S. 2013, *ApJ*, 764, 50
- Lopez, L. A., Ramirez-Ruiz, E., Huppenkothen, D., Badenes, C., & Pooley, D. A. 2011, *ApJ*, 732, 114
- López-Coto, R., Carmona, E., Bednarek, W., Blanch, O., Cortina, Juan., Wilhelmi, E., Torres, D., Martin, J., Pérez-Torres, M. Á 2016, *European Physical Journal Web of Conferences*, 121, 04007
- Lyubarsky, Y. E. 2012, *MNRAS*, 427, 1497
- MacFadyen, A. I., Woosley, S. E., & Heger, A. 2001, *ApJ*, 550, 410
- Maund, J. R., Wheeler, J. C., Patat, F., Baade, D., Wang, L., Höflich, P. 2007, *MNRAS*, 381, 201
- Meier, D. L., Epstein, R. I., Arnett, W. D., & Schramm, D. N. 1976, *ApJ*, 204, 869

- Miceli, M., Orlando, S., Reale, F., Bocchino, F., & Peres, G. 2013, *MNRAS*, 430, 2864
- Milisavljevic, D., Soderberg, A. M., Margutti, R., et al. 2013, *ApJ*, 770, LL38
- Morris, T., & Podsiadlowski, P. 2009, *MNRAS*, 399, 515
- Mösta, P., Richers, S., Ott, C. D., et al. 2014, *ApJ*, 785, LL29
- Müller, B. 2016, arXiv:1608.03274
- Ng, C.-Y., Romani, R. W., Briskin, W. F., Chatterjee, S., & Kramer, M. 2007, *ApJ*, 654, 487
- Olmi, B., Del Zanna, L., Amato, E., Bucciantini, N., & Mignone, A. 2016, arXiv:1610.07956
- Oonk, J. B. R., van Weeren, R. J., Salas, P., Salgado, F., Morabito, L. K., Toribio, M. C., Tielens, A. G. G. M., Röttgering, H. J. A. 2016, arXiv:1609.06857
- Papish, O., Nordhaus, J., & Soker, N. 2015, *MNRAS*, 448, 2362
- Papish, O., & Soker, N. 2014a, *MNRAS*, 438, 1027
- Papish, O., & Soker, N. 2014b, *MNRAS*, 443, 664
- Papish, O., & Soker, N. 2011, *MNRAS*, 416, 1697
- Podsiadlowski, P., Joss, P. C., & Rappaport, S. 1990, *A&A*, 227, L9
- Reynoso, E. M., & Walsh, A. J. 2015, *MNRAS*, 451, 3044
- Safi-Harb, S., Ribó, M., Butt, Y., Matheson, H., Negueruela, I., Lu, F., Jia, S., & Chen, Y. 2007, *ApJ*, 659, 407
- Safi-Harb, S., & Petre, R. 1999, *ApJ*, 512, 784
- Sari, R., & Piran, T. 1997, *ApJ*, 485, 270
- Schenck, A., & Park, S., & Burrows, D., & Hughes, J., & Lee, J., & Mori, K. 2014, *ApJ*, 791,50
- Seward, F. D., Tucker, W. H., & Fesen, R. A. 2006, *ApJ*, 652, 1277
- Shaviv, N. J., & Dar, A. 1995, *ApJ*, 447, 863
- Shelton, R., & Kuntz, K., & Petre, R. 2004, *ApJ*, 611, 906
- Shibanov, Y. A., Lundqvist, N., Lundqvist, P., Sollerman, J., & Zyuzin, D. 2008, *A&A*, 486, 273
- Shiber, S., Kashi, A., & Soker, N. 2016, arXiv:1607.00839
- Slane, P., & Helfand, D., & Swaluw, E., & Murray, S. 2004, *ApJ*, 616, 403
- Soker, N. 2016a, *New A*, 47, 88
- Soker, N. 2016b, *New Astronomy Reviews*, in press, arXiv:1605.02672
- Sukhbold, T., Ertl, T., Woosley, S. E., Brown, J. M., & Janka, H.-T. 2016, *ApJ*, 821, 38
- Sukhbold, T., & Woosley, S. E. 2016, *ApJ*, 820, L38

- Takiwaki, T., & Kotake, K. 2011, *ApJ*, 743, 30
- Tanaka, T. 2009, International Cosmic Ray Conference
- Temim, T., Gehrz, R. D., Woodward, C. E., et al. 2006, *AJ*, 132, 1610
- Tocknell, J., De Marco, O., & Wardle, M. 2014, *MNRAS*, 439, 2014
- Tsebrenko, D., & Soker, N. 2015b, *MNRAS*, 450, 1399
- Tsebrenko, D., & Soker, N. 2015a, *MNRAS*, 447, 2568
- Tsebrenko, D., & Soker, N. 2013, *MNRAS*, 435, 320
- Wilson, J. R. 1985, *Numerical Astrophysics*, 422
- Woosley, S. E. 1993, *Bulletin of the American Astronomical Society*, 25, 55.05
- Woosley, S., & Janka, T. 2005, *Nature Physics*, 1, 147
- Yang, H., & Chevalier, R. A. 2015, *ApJ*, 806, 153